Research Article

Quantitative microstructure study of melt-spun $Mg_{65}Cu_{25}Y_{10}$

Alexander Katz-Demyanetz[1] · Menachem Bamberger[2] · Michael Regev[3]

Received: 28 May 2020 / Accepted: 16 September 2020 / Published online: 11 October 2020

Abstract

$Mg_{65}Cu_{25}Y_{10}$ ribbons were produced by melt spinning. XRD, DSC, HRSEM and HRTEM were used to investigate their microstructure in its as-cast condition as well as after 3- and 6-minute exposures to 100 °C, 120 °C, 150 °C, 200 °C and 300 °C. XRD and DSC studies showed that the as-cast material had an amorphous character; the HRTEM investigation revealed that although the as-cast $Mg_{65}Cu_{25}Y_{10}$ is known to be one of the best glass formers, it is nano-crystalline rather than amorphous. The fraction of the crystalline phase after each treatment was calculated by means of quantitative analysis that took into account the degree of crystallinity of the as-cast material as revealed by HRTEM. The current study showed that quantitative analysis may lead to serious errors when relying on the absence of crystalline peaks in the XRD spectrum as if the material is completely amorphous. Moreover, it seems that HRTEM examination is essential for carrying out quantitative XRD and DSC analyses.

✉ Michael Regev, michaelr@braude.ac.il; Alexander Katz-Demyanetz, kalexand@trdf.technion.ac.il; Menachem Bamberger, mtrbam@technion.ac.il | [1]Foundry Laboratory, Israel Institute of Metals, Technion – Israel Institute of Technology, Haifa, Israel. [2]Department of Materials Science and Engineering, Technion – Institute of Technology, Haifa, Israel. [3]Mechanical Engineering Department, ORT Braude College of Engineering, P.O.B. 78, Karmiel, Israel.

SN Applied Sciences (2020) 2:1811 | https://doi.org/10.1007/s42452-020-03522-3

Graphic abstract

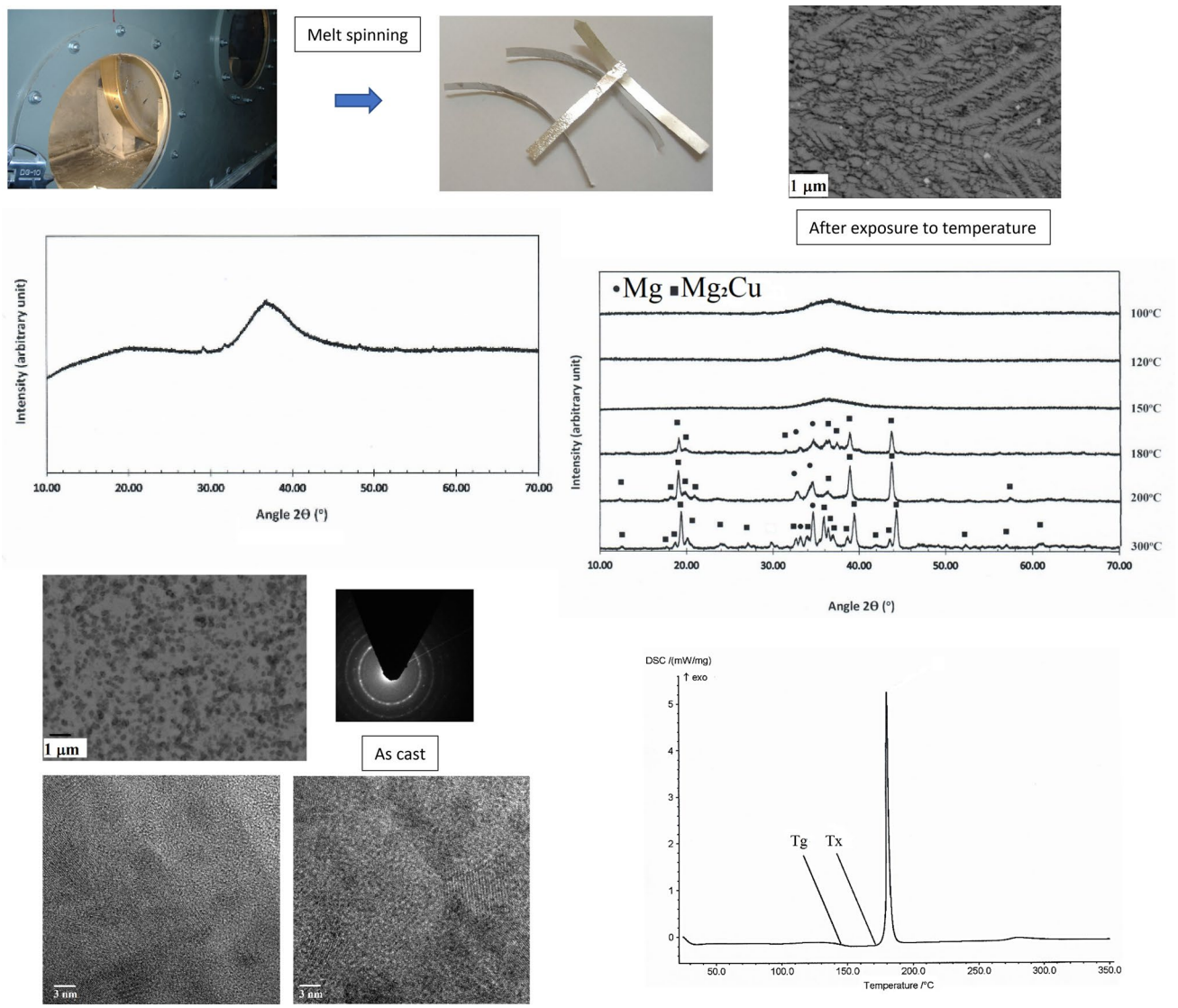

Keywords $Mg_{65}Cu_{25}Y_{10}$ · Melt spinning · Metallic glass · HRTEM · XRD · DSC

1 Introduction

Magnesium alloys are characterized by good physical properties: they exhibit high strength, are lightweight, and have good damping absorption and good thermal and electrical conductivity. Amorphous magnesium alloys, moreover, exhibit higher strength, hardness, and a large elastic domain in addition to having excellent corrosion resistance. Among the various existing magnesium alloys, the Mg–Cu–Y system is known to be one of the best glass formers. The $Mg_{65}Cu_{25}Y_{10}$ was reported in early publications of Inoue et al. [1–3], who pointed at Cu content of 25 at. % and Y content of 10 at. % as optimal for high Glass Forming Ability (GFA) so that BMG rods with a diameter of 4 mm could be produced by copper mold casting. This high GFA is due to the lowest critical cooling rate and the largest temperature span of the supercooled region (ΔT_x) in the Mg–Cu–Y system, both achieved with the $Mg_{65}Cu_{25}Y_{10}$ composition and equal 93 K/s and 60 °C, respectively. The temperature span of the supercooled region is defined as follows:

$$\Delta T_x = \left(T_x - T_g\right) \quad (1)$$

where ΔT_x The temperature span of the supercooled region [°C], T_x Crystallization temperature [°C], T_g Melt-glass transition temperature [°C]

Being such a good glass former, the $Mg_{65}Cu_{25}Y_{10}$ composition has therefore been studied extensively [1–21]. These investigations were conducted on amorphous $Mg_{65}Cu_{25}Y_{10}$ obtained by different casting processes, namely, pressure die-casting [1, 2, 4], injection into a copper mold [6–13], injection into a water-cooled Cu mold [14], melt spinning [15–20], rapid quenching without listing the exact process [21, 22] and permanent mold without stating anything about the mold [23]. The characterization techniques used in order to determine the amorphous structure of the $Mg_{65}Cu_{25}Y_{10}$ alloy included X-ray diffraction (XRD) [1, 4, 6–23], differential scanning calorimetry (DSC) [1, 2, 4, 6–8, 10–18, 22, 23] and transmission electron microscopy (TEM) [1, 6, 8, 9, 13, 16, 18, 21]. All the studies that examined the microstructure of $Mg_{65}Cu_{25}Y_{10}$ seem to agree that sufficiently rapid cooling rates during the casting process of this composition yield a fully amorphous structure. It should be noticed that only two references [19, 20] include high-resolution transmission electron microscopy (HRTEM) of $Mg_{65}Cu_{25}Y_{10}$; however, these HRTEM studies deal with the characterization of nanoporous structures obtained by selective dissolution of amorphous $Mg_{65}Cu_{25}Y_{10}$ and not with the degree of amorphization of the alloy.

In a previous study by Regev et al. [24], high-resolution transmission electron microscopy (HRTEM) as well as other characterization tools, namely, XRD, DSC and high-resolution scanning electron microscope (HRSEM), were applied in order to study the amorphous nature of melt-spun $Mg_{65}Cu_{25}Y_{10}$. This study [24] also included XRD investigations of $Mg_{65}Cu_{25}Y_{10}$ after 5-minute exposure to 50 °C, 100 °C, 150 °C and 200 °C. The study found that the material lost its amorphous character upon exposure to temperature; however, this conclusion was based solely on XRD peak identification without any quantitative analysis. Another important finding was that according to XRD and DSC, the $Mg_{65}Cu_{25}Y_{10}$ in its as-cast state was found to be amorphous, while HRTEM study showed that it was nano-crystalline with an average grain size of about 8 nm. The proposed qualitative explanation was that the material was indeed nano-crystalline while the amorphous character of the XRD and DSC spectra was due to the large contribution of the grain boundaries, which are amorphous by definition.

The current paper offers a quantitative approach for calculating the volume fraction of the crystalline phase in the case of melt-spun $Mg_{65}Cu_{25}Y_{10}$ specimens that had been exposed to 100 °C, 120 °C, 150 °C, 180 °C, 200 °C and 300 °C for 3 and 6 min and hence crystallized to various degrees prior to the DSC and XRD studies. In addition, the corrections required by the existence of the nano-crystalline phase in the as-cast material, as revealed by HRTEM, were introduced and their influence on the accuracy of the quantitative analysis is discussed.

2 Materials and methods

The chemical composition studied was, as mentioned above, $Mg_{65}Cu_{25}Y_{10}$. Pure Mg (99.9 wt % purity) and Cu (99.97 wt % purity) metals and an Mg-40 wt % Y master alloy with degree of purity of 99.9 wt % for both Mg and Y were used for the alloy preparation. Alloying was carried out in a graphite crucible under an Ar protective atmosphere. The materials blend was melted and then

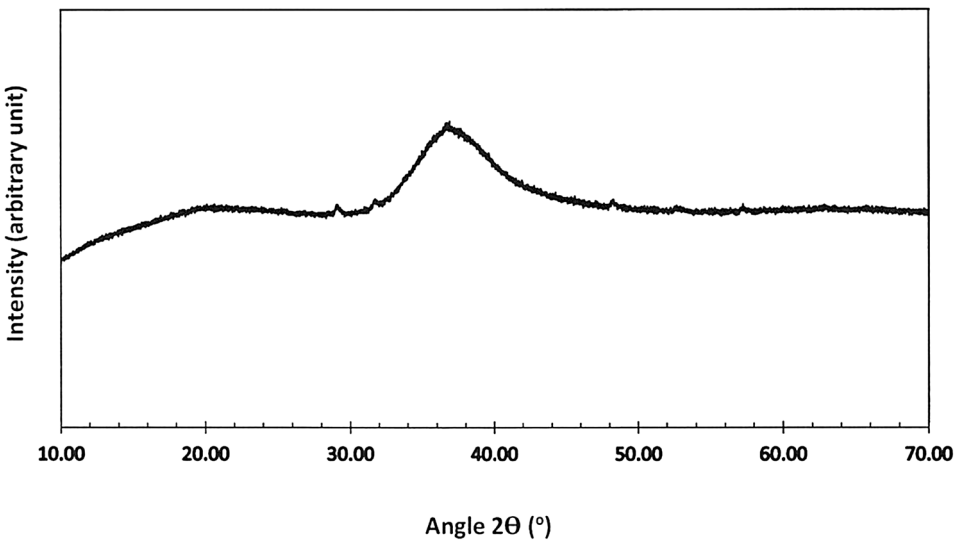

Fig. 1 An XRD spectrum of the melt-spun $Mg_{65}Cu_{25}Y_{10}$ in its as-cast condition

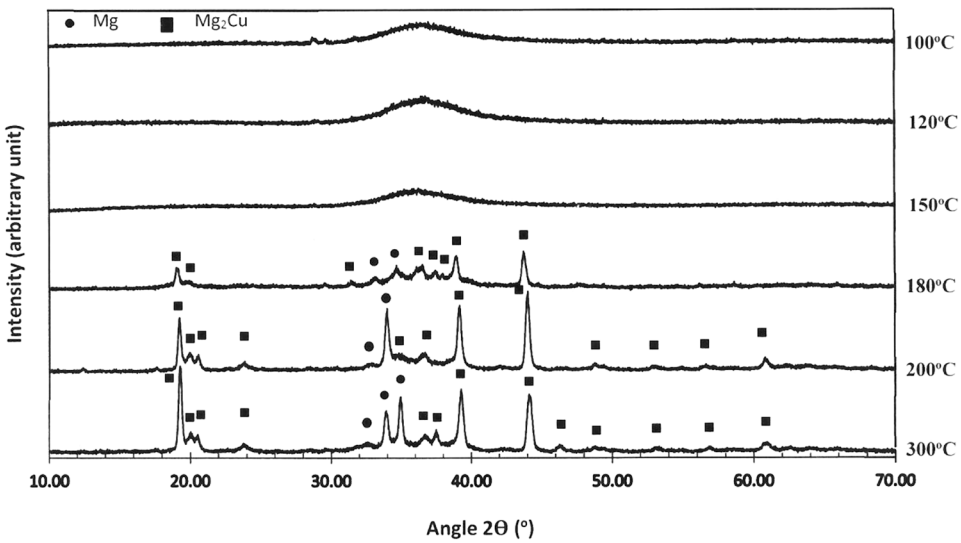

Fig. 2 XRD spectra of the melt -spun $Mg_{65}Cu_{25}Y_{10}$ after 3-minute-long exposures to various temperatures

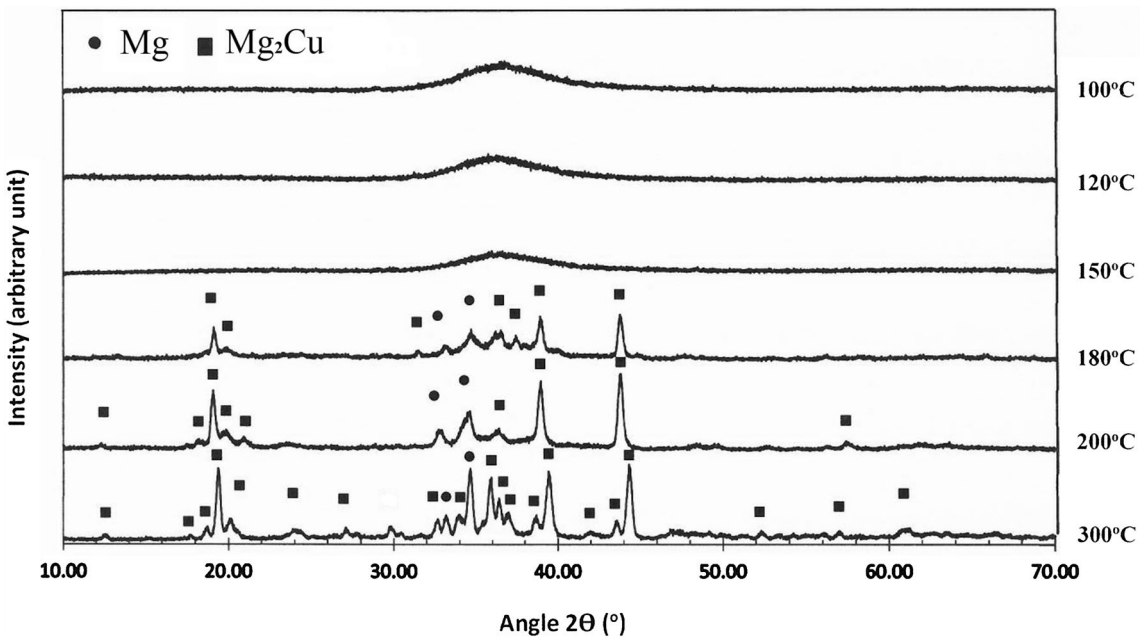

Fig. 3 XRD spectra of the melt-spun $Mg_{65}Cu_{25}Y_{10}$ after 6-minute-long exposures to various temperatures

homogenized at 800 °C for 1 h under an Ar protective atmosphere before casting. The alloy was then re-melted and cast by a melt-spinning machine with a brass drum rotating at 1000 rpm having linear velocity of about 42 m/s. The final product was ~ 80-µm-thick ribbons. These $Mg_{65}Cu_{25}Y_{10}$ ribbons then underwent 3 and 6 min exposure to 100 °C, 120 °C, 150 °C, 180 °C, 200 °C and 300 °C in Ar atmosphere. Keeping in mind that the amorphous structure is expected to crystallize during heating, the reason for selecting different temperatures and time intervals was to study the character of the crystallization process, namely, how long it takes and to what extent under given conditions. A 0.2 mm-thick K-type thermocouple was attached to each sample, the sample was then put in an oven, between two hot massive steel plates, both the oven and the plates had been previously heated to the desired temperature. Cooling was conducted also between two cold massive steel plates placed outside the oven. The temperature was recorded using a National Instruments LTD measuring computerized system. The measured heating/cooling rates were approximately 1000 °C/s.

XRD tests were performed using Stationary Rigaku Smart Lab diffractometer equipped with a Cu tube ($\lambda_{K\alpha} = 1.5406$ Å), and the measurement step was 0.01° with

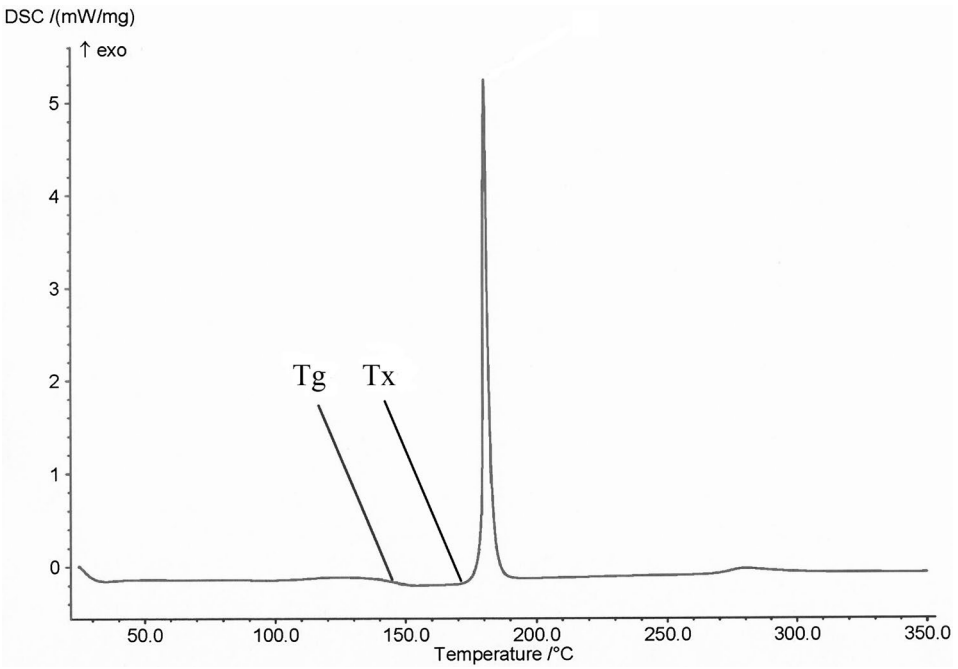

Fig. 4 A DSC curve of the as-cast melt-spun $Mg_{65}Cu_{25}Y_{10}$

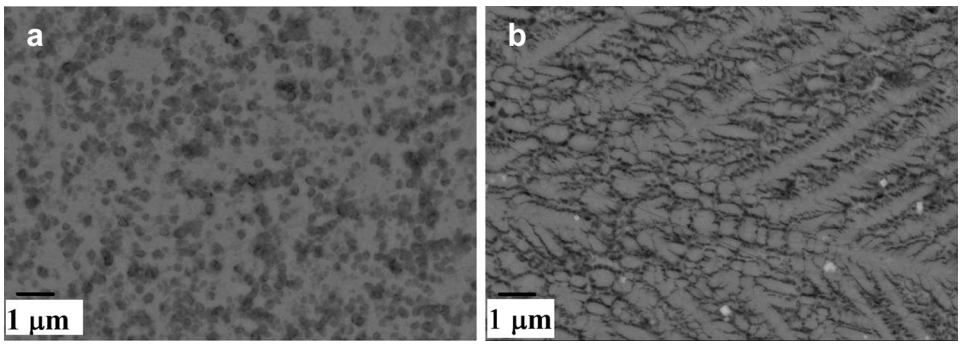

Fig. 5 HRSEM micrographs of **a** As-cast melt-spun $Mg_{65}Cu_{25}Y_{10}$; **b** after 5 min at 200 °C

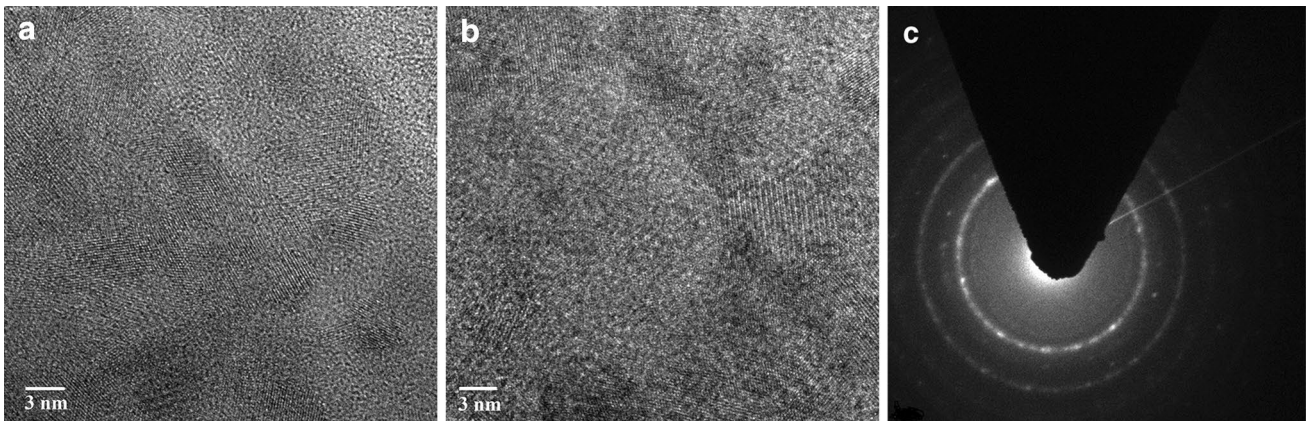

Fig. 6 HRTEM image of the as-cast melt-spun $Mg_{65}Cu_{25}Y_{10}$: **a,b** images; **c** SADP with aperture diameter—200 nm

exposure time of 1 s per step. The melt-spun specimen was ground to powder having an average particle size of about the thickness of the ribbon (~80 µm) prior to the XRD tests in order to eliminate any texture influence. The microstructure was studied under a Zeiss Ultra Plus high-resolution scanning electron microscope (HRSEM), HRTEM investigation was conducted using an FEI Titan 300 kV HRTEM. TEM specimens were prepared by using a Helios NanoLab G3 FEI FIB (Focused Ion Beam).

The DSC study summarized in the current paper is based on scanning experiments. The melt-spun specimens were heated using a DSC 204F1 Phoenix calorimeter at a constant rate of 10 °C/min until they reached 700 °C.

3 Results

Figure 1 depicts an XRD spectrum of the melt-spun $Mg_{65}Cu_{25}Y_{10}$ in its as-cast condition, while Figs. 2 and 3, respectively, depict XRD spectra of the melt-spun $Mg_{65}Cu_{25}Y_{10}$ after 3- and 6-minute-long exposures to various temperatures.

As can be seen from Fig. 1, the spectrum has an amorphous character, while Figs. 2 and 3 show that the amorphous character of the melt-spun material disappeared completely after 3- or 6-minute-long exposures to 180 °C and that the spectra appear to be crystalline.

A DSC curve of the as-cast melt-spun $Mg_{65}Cu_{25}Y_{10}$ is presented in Fig. 4, the glass transition temperature (T_g) and the crystallization temperature (T_x) are shown.

HRSEM micrographs showing the microstructural changes during exposure to temperature are given in Fig. 5a and b, and these micrographs were taken using both secondary and back-scattered detectors. In the case of the as-cast melt-spun $Mg_{65}Cu_{25}Y_{10}$ (Fig. 5a), no grain structure is discernible while dendritic morphology and crystalline structure can be clearly seen in Fig. 5b which was taken after 5 min at 200 °C. The content of all three alloying elements (Mg, Cu and Y) was recorded in the matrix of the grains in all examined samples by means of Electron Probe Micro-Analysis (EPMA).

A HRTEM BF image of the as-cast material is shown in Fig. 6a,b, while a diffraction pattern is shown in Fig. 6c. The nano-crystalline character can be clearly observed in Fig. 6a, while the ring selected area diffraction pattern (SADP) shown in Fig. 6b, which is obtained from the region shown in Fig. 6a, supports this claim. Other examples of single nano-grains have been already published elsewhere [24]. Examination of a few tens of nano-grains leads to the estimation that the average grain size of the as-cast material is about 8 nm, while the width of the grain boundary region is about 2 nm (10–15 times the magnesium lattice parameter). Thus, the volume fraction of the grain boundaries turns out to be about 70%.

Table 1 DSC results

Temperature and duration of exposure	T_g, °C	T_x, °C	ΔH_m, J/g	ΔH_c, J/g
As-cast	138	179.4	92.18	92.18
100 °C—3 min	137.7	188.3	102.49	85.90
120 °C—3 min	136.3	189.8	97.26	78.82
150 °C—3 min	136.7	185.5	91.14	69.94
180 °C—3 min	140.2	178.6	88.52	5.56
200 °C—3 min	–	–	87.57	0
300 °C—3 min	–	–	92.18	0
100 °C—6 min	138	185.4	83.34	78.73
120 °C—6 min	136	189.8	86.48	73.57
150 °C—6 min	137.8	185.1	88.36	66.24
180 °C—6 min	139	181.2	92.73	5.16
200 °C—6 min	–	–	88.49	0
300 °C—6 min	–	–	92.18	0

4 Discussion

Figures 2 and 3 show that two crystalline phases were identified by XRD, namely, Mg and Mg_2Cu, keeping in mind that the alloy contains 10 at. % Y, the appearance of an Y containing crystalline phase after exposure to temperature is expected. It may be claimed that the unidentified peak around 2=29.5° (see Fig. 3) belongs to $Mg_{24}Y_5$. However, the existence of $Mg_{24}Y_5$ crystalline phase requires at least two other strong peaks at 2=19.3° and at 2=33.7°. As for the expected peak at 2=19.3°—there is a peak of Mg_2Cu at the same angle while in the case of 2=33.7° there is close peak of Mg at 2=34.4°, keeping in mind that small shift of certain peaks cannot be excluded, it is not clear whether this peak belongs to Mg or to $Mg_{24}Y_5$. Moreover, the intensity of the peak at 2=19.3° is expected to be more than five times higher than that of the 2=33.7° peak while Fig. 3 shows the opposite situation. Referring to EDS analysis, it should be noted that no Y rich phase was detected by EDS whatsoever while the Y content was found to be similar to that of the nominal composition. In summary, the authors feel that it cannot be unambiguously concluded that $Mg_{24}Y_5$ phase does crystallize after exposure to temperature.

The DSC curves of the melt-spun $Mg_{65}Cu_{25}Y_{10}$ after 3- and 6-minute-long exposures to 100 °C, 120 °C, 150 °C, 180 °C, 200 °C and 300 °C are analyzed in the same manner Fig. 4 and were analyzed, namely, T_g and T_x were detected and the enthalpy variation during the crystallization was calculated by integrating the curve in the vicinity of the crystallization peak. The values of T_g, T_x and the enthalpy variations during the crystallization and melting processes

are summarized in Table 1. The mentioned enthalpies are actually integral intensities (calculated by DSC 204Fi Phoenix built-in software) of the corresponding DSC peaks.

Comparing the crystallization behavior observed in the current study with some other DSC studies reported over the last few years [4, 25–27] it comes that the current study is in line with some of the reported results of other researchers. The value of T_x for the as-cast material, as can be seen from Table 1, is 179.4 °C and the value of ΔT_x obtained is 41.4 °C. Kiljan et al. [4] who studied 1-mm-thick $Mg_{65}Cu_{25}Y_{10}$ BMG plates produced by pressure die-casting reported about T_g varying between 122 and 141 °C, T_x varying between 180 and 187 °C, and ΔT_x varying, therefore, between 43 and 58 °C which is closer to ΔT_x obtained in the current study than to the value of 60 °C reported by Inoue et al. [1]. Arison Kung et al. [25] produced $Mg_{65}Cu_{25}Y_{10}$ BMG by both melt spinning and spray cooling, they reported about $T_g = 155$ °C, $T_x = 216$ °C and $\Delta T_x = 61$ °C in the case of melt spinning while for the BMG produced by spray cooling the values of T_g, T_x and ΔT_x were 142–151 °C, 213–220 °C and 69–71 °C, respectively. Their reported results for ΔT_x are closer to those reported by Inoue et al. [1] than to the results of the current study. Ismail et al. [26] studied crystallization of $Mg_{58}Cu_{31}Gd_{11}$ BMG by means of DSC and XRD. Although studying a different composition, they noted the appearance and growth Mg_2Cu phase accompanying the crystallization process, the first stage of which started at 178 °C, and the second one started at 220 °C, the existence of Mg_2Cu phase is well supported by the current study. Rozenberg et al. [27] studied rapidly solidified Mg-Cu-RE alloys, they pointed at the positive role of Y on the GFA of such alloys and found that for the $Mg_{65}Cu_{25}Y_{10}$ alloy, T_x was 184 °C and T_g was 152 °C so that ΔT_x was found to be 32 °C.

As stated earlier, examination of a few tens of nano-grains leads to the estimation that the average grain size of the as-cast material is about 8 nm, while the width of the grain boundary region is about 2 nm, under the assumption that the grains are spherical the volume of an average grain without its boundary was found to be 268 nm^3 while adding the volume of the grain boundary the total volume comes to 904 nm^3. Thus, the volume fraction of the grain boundaries turns out to be about 70%.

One question that may be asked at this point is whether the loss of the amorphous character is not caused by specimen preparation process or due to heating by the electron beam at the TEM specimen chamber. When referring to this question one should keep in mind that the specimen, being metallic, is characterized by very high thermal conductivity. The temperature rise during preparation by FEI Helios NanoLab FIB at the highest beam density was calculated by Ishitani and Kaga [28] and was found to vary between 6.6 °C for aluminum and 17.7 °C for stainless steel. For the sake of comparison, the temperature rise of SiO_2 under the same conditions is more than 800 °C according their calculations [28]. As for the temperature increase due to the electron beam at the TEM specimen chamber, the authors assume that it did not reach T_x due to the same reason of high thermal conductivity. Experimental result which supports this claim can be obtained from Fig. 5b which was taken after 5 min at 200 °C. Keeping in mind that T_x was found to be between 179.9 and 197.2 °C, one can see from Fig. 5b that the grain size in the case of 5-min-long exposure to 200 °C is at the order of magnitude of 1 µm, a hundred times coarser than the nano-grains detected by HRTEM. Taking into account that a typical HRTEM study took at least three hours and that no change in grain size was detected, namely, the grains remained at the size of 8 nm, it can be concluded that the specimen's temperature did not reach the glass transition temperature.

Calculations of the percentage of the crystalline phases were based on two independent techniques, namely, XRD and DSC. Quantitative analysis of XRD spectra enables to estimate the weight fraction of each phase by comparing the intensities obtained from the different phases, given that the peak intensity of a certain phase is proportional to its weight fraction. Consequently, this analysis requires a reference specimen of the pure phase under study. Since no crystalline reflections were revealed by XRD in the as-cast sample, it was first assumed to be completely amorphous and the integral intensity of its dome-shaped spectrum was taken as an "amorphous reference" [29–34]. In the case of partially crystallized samples, the integral intensities of each of the crystalline reflections were measured and summarized and then divided by the integral intensity of that of the dome-shaped amorphous Ref. [35].

Table 2 Degree of crystallinity after exposure to temperature based on XRD analysis

Temperature and duration of exposure	Crystallinity percentage without correction	Corrected crystallinity percentage
100 °C—3 min	24	47
120 °C—3 min	27	49
150 °C—3 min	32	52
180 °C—3 min	80	86
200 °C—3 min	91	94
300 °C—3 min	100	100
100 °C—6 min	10	37
120 °C—6 min	19	43
150 °C—6 min	34	54
180 °C—6 min	81	87
200 °C—6 min	93	95
300 °C—6 min	100	100

The weight fraction of the phase under study was calculated as follows [36]:

$$W_\alpha = \frac{\left(\frac{I_\alpha}{I_{\alpha-\text{pure}}}\right)\left(\frac{\mu}{\rho}\right)_\beta}{\left(\frac{\mu}{\rho}\right)_\alpha - \left(\left(\frac{\mu}{\rho}\right)_\alpha - \left(\frac{\mu}{\rho}\right)_\beta\right).\left(\frac{I_\alpha}{I_{\alpha-\text{pure}}}\right)} \quad (2)$$

where W_α weight fraction α phase in the specimen, μ linear absorption coefficient [cm^{-1}], ρ density [gr/cm^3], α, β Mg and Mg_2Cu phases, respectively, I_α intensity of α phase peak, $I_{\alpha-\text{pure}}$ intensity of α phase peak in a pure α specimen

The ratio $\frac{\mu}{\rho}$ is known as the mass attenuation coefficient, in the considered case its values are close for both the amorphous and for the two crystalizing phases (Mg and Mg_2Cu). Since the chemical composition of the revealed crystalline phases were identified, their attenuation coefficients are known, these values are quite close, hence, Eq. 2 can be simplified to:

$$W_\alpha = \left(\frac{I_\alpha}{I_{\alpha-\text{pure}}}\right) \quad (3)$$

Calculation of the percentage of crystalline phase in nano-amorphous mixture by means of qualitative XRD analysis is not new, for example, Abrosimova et al. [37] reported on $Fe_{73.9}B1_{3.2}Si_{10.9}C_2$ bulk metallic glass synthesized and quantitatively examined by XRD. Their calculation method was based on peaks integral intensities ratio. As a part of their technique and in order to take into account the difference in the absorptions of the examined crystalline/amorphous phases, an intensities ratio vs. real concentrations calibration curve was constructed.

Table 3 Degree of crystallinity after exposure to temperature based on DSC analysis

Temperature and duration of exposure	Crystallinity percentage without correction	Corrected crystallinity percentage
100 °C—3 min	18	43
120 °C—3 min	20	44
150 °C—3 min	23	46
180 °C—3 min	90	93
200 °C—3 min	95	96
300 °C—3 min	100	100
100 °C—6 min	5	33
120 °C—6 min	14	40
150 °C—6 min	24	47
180 °C—6 min	95	96
200 °C—6 min	96	97
300 °C—6 min	100	100

In the current study, after the weight fraction of the crystalline phase had been calculated according to Eq. 3, it was then corrected by taking into account the HRTEM findings, namely, that the amorphous reference contained only 70% amorphous phase. The XRD results are summarized in Table 2.

It should be noted that several small crystalline reflections are discernible in the spectrum shown in Fig. 1 in the vicinity of 29°, 32°, 48° and 58°. Applying the procedure described above on these peaks, one can see that the overall contribution of these phases is around the detection limit of the XRD system and does not affect the quantitative assessment made and discussed in the current paper. Moreover, the lack of appearance of these small reflections in the spectra corresponding to heat treatments at 120 °C and 150 °C and the fact that these reflections do not fit any crystalline reflection obtained at the thermally treated specimens support the claim that these peaks can be referred as a minor heterogeneity of the as-cast ribbon, probably due to metastable phases formed during casting.

DSC pattern analyses were conducted on the basis of the following expression which was originally developed for polymers [38] and was applied successfully on bulk metallic glasses (BMGs) as well [35].

$$\text{pc} = \frac{\Delta H_\text{m} - \Delta H_\text{c}}{\Delta H_\text{m}^0} * 100\% \quad (4)$$

where pc percentage calculation, ΔH_m melting enthalpy, ΔH_C crystallization enthalpy, ΔH_m^0 melting enthalpy of the completely amorphous reference sample

The above analysis was first conducted under the assumption that the as-cast melt-spun sample was completely amorphous. Then it was further modified by introducing the corrections required due to the existence of the nano-crystalline phase of the as-cast material, as revealed by HRTEM. The quantitative results of this analysis are given in Table 3.

A comparison between the crystallinity percentage as calculated according to XRD (Table 1) and that calculated according to DSC (Table 2) indicates that the difference does not exceed a few percentage points, especially in the case of the corrected crystallinity percentage. The maximum difference was obtained in the case of 6-min exposure to 180 °C, in which the crystallinity percentage was found to be 87% according to XRD versus 96% according to DSC. Yet, these differences are inconsistent because the crystallinity percentage as calculated according to XRD is higher in the cases of 100 °C, 120 °C and 150 °C compared to that obtained by applying quantitative analysis on the DSC results, while in the cases of 180 °C and 200 °C DSC yielded a higher crystallinity percentage. According to XRD and DSC, the as-cast melt-spun $Mg_{65}Cu_{25}Y_{10}$ seems to be

amorphous, while clear nano-grains were observed by means of HRTEM. As proposed elsewhere by Regev et al. [24], the contribution of the grain boundaries, which are amorphous by definition, is responsible for the amorphous character of the XRD spectrum. Tables 2 and 3 show that serious errors may occur when regarding the as-cast melt-spun $Mg_{65}Cu_{25}Y_{10}$ as completely amorphous. In turn, this shows the limitations of relying solely on XRD analysis. Keeping in mind that $Mg_{65}Cu_{25}Y_{10}$ is known to be one of the best glass formers, the general question left to be answered is whether there are "true" amorphous materials or whether crystallinity will always be revealed under sufficiently high resolution. Nevertheless, the described quantitative analysis shows that, at least in the current case, using HRTEM combined with XRD and DSC analyses is essential in order to avoid serious errors. This conclusion is supported by the work of Gloriant et al. [39] who reported on evaluation of the volume fraction crystallized during devitrification of Al-based amorphous alloys. They applied XRD and DSC examination techniques and relied on the ratio of the integral intensities of the relevant peaks of crystalline and amorphous phases. They concluded that the use of DSC and XRD techniques for evaluating the percentage of crystalline phase in a nano-amorphous mixture is not straightforward, and hence, appropriate correction factors should be applied for better estimation.

5 Conclusions

- The microstructure of melt-spun $Mg_{65}Cu_{25}Y_{10}$ in its as-cast condition as well as after 3- and 6-minute exposures to 100 °C, 120 °C, 150 °C, 200 °C and 300 °C was investigated by means of XRD, DSC, HRSEM and HRTEM.
- Quantitative analysis was conducted on both XRD and DSC results in order to estimate the fraction of the crystalline phase after each thermal treatment. The difference between these two independent analyses did not exceed a few percentage points.
- Further improvement in the quantitative analysis was achieved by taking into account the degree of crystallinity of the as-cast material as revealed by HRTEM.
- The XRD spectrum obtained in the current study in the case of the melt-spun as-cast material appeared to be amorphous even though the material contained about 30% of crystalline phase. This shows, in turn, that visual inspection of the XRD spectrum was not sufficient in the current case to decide about the material being completely amorphous.
- The current study showed that quantitative analysis might have lead to serious errors if the material had been assumed to be completely amorphous relying on the absence of crystalline peaks in the XRD spectrum.

Acknowledgments The authors wish to thank Mr. Eyal Eshed for his assistance with the DSC study. Thanks are also due to Ms. Alexandra Rozhitsky and to Ms. Shakhar Josefson for taking part in the experimental work and analysis.

Compliance with ethical standards

Conflict of interest On behalf of all authors, the corresponding author states that there is no conflict of interest.

References

1. Inoue A, Kato A, Zhang T, Kim SG, Masumoto T (1991) Mg-Cu–Y amorphous alloys with high mechanical strengths produced by a metallic mold casting method. Mater Trans, JIM 32:609
2. Inoue A, Nakamura T, Nishiyama N, Masumoto T (1992) Mg–Cu–Y bulk amorphous alloys with high tensile strength produced by a high-pressure die casting method. Mater Trans, JIM 33:937
3. Inoue A, Masumoto T (1993) Mg-based amorphous alloys. Mater Sci Eng, A 173:1
4. Kiljan A, Nowosielski R, Babilas R (2017) Properties and structures of bulk metallic glasses based on magnesium. Mater Technol 51:563
5. Inoue A (2000) Stabilization of metallic supercooled liquid and bulk amorphous alloys. Acta Mater 48:279
6. Gun B, Laws KJ, Ferry M (2006) Static and dynamic crystallization in Mg–Cu–Y bulk metallic glass. J Non-Cryst Solids 352:3887
7. Park ES, Kang HG, Kim WT, Kim DH, Non-Cryst J (2001) The effect of Ag addition on the glass-forming ability of Mg–Cu–Y metallic glass alloys. J Non-Cryst Solids 279:154
8. Gun B, Laws KJ, Ferry M (2007) Elevated temperature flow behaviour of a Mg-based bulk metallic glass. Mater Sci Eng, A 471:130
9. Huang K, Chen G, Zhao Y, Wang G, Shao Y (2012) Crystallization microstructure of $Mg_{65}Cu_{25}Y_{10}$ bulk amorphous alloy. Trans Nonferrous Met Soc China 22:831
10. Gun B, Laws KJ, Ferry M (2010) Viscosity-related properties of $Mg_{65}Cu_{25}Y_{10}$ bulk metallic glass determined by uniaxial tension in the supercooled liquid region. J. Alloys Comp. 496:582
11. Men H, Hu ZQ, Xu J (2002) Bulk metallic glass formation in the Mg–Cu–Zn–Y system. Scripta Mater 46:699
12. Gun B, Laws KJ, Ferry M (2006) Superplastic flow of a Mg-based bulk metallic glass in the supercooled liquid region. J Non-Cryst Solids 352:3896
13. Zhang J, Zhang HF, Quan MX, Hu ZQ (2003) Effect of pressure on thermal stability of $Mg_{65}Cu_{25}Y_{10}$ bulk metallic glass. Scripta Mater 49:485
14. Li ZG, Hui X, Zhang CM, Wang ML, Chen GL (2007) Strengthening and toughening of Mg–Cu–(Y, Gd) bulk metallic glasses by minor addition of Be. Matter. Lett. 61:5018
15. Satta M, Palumbo M, Rizzi P, Baricco M (2007) Ternary compounds and glass formation in the Cu-Mg-Y System. Adv Eng Mater 9:475
16. Gebert A, Khorkounov B, Wolff U, Mickel Ch, Uhlemann M, Schultz L (2006) Stability of rapidly quenched and hydrogenated

Mg–Ni–Y and Mg–Cu–Y alloys in extreme alkaline medium. J. Alloys Comp. 419:319
17. Hung TH, Chang YC, Wang YN, Tang CW, Kuo JN, Chen HM, Tsai YL, Huang JC, Jang JSC, Liu CT (2007) Development of Mg based amorphous alloys with higher amounts of rare earth elements. Mater Trans, JIM 48:1621
18. Savyak MP, Gebert A, Uhlemann M (2004) Effect of hydrogen on the amorphous structure of the alloy $Mg_{65}Cu_{25}Y_{10}$ under electrochemical saturation. Powder Metall Met Ceram 43:513
19. Xu H, Pang S, Jin Y, Zhang T (2016) General synthesis of sponge-like ultrafine nanoporous metals by dealloying in citric acid. Nano Res. 9:2467
20. Qin F, Dan Z, Hara N, Li W, Li Y (2016) Selective dissolution of an amorphous $Mg_{65}Cu_{25}Y_{10}$ alloy in organic acids and dilute HCl solution. Mater Chem Phys 179:27
21. Du C, Qi H, Yan B, Guan L (2010) Preparation, structure and properties of Mg-based bulk amorphous and nanocrystalline nanomaterials. In: Proceedings INEC 2010, Hong Kong, China: IEEE. https://doi.org/10.1109/inec.2010.5425144
22. Savyak MP (2006) Thermal stability of amorphous alloys $Mg_{65}Cu_{25}Y_{10}$, $Mg_{63}Ni_{30}Y_7$ after electrochemical hydrogen absorption. Powder Metall Met Ceram 45:196
23. Chen G, Ferry M (2007) Crystallization and thermally induced surface relief effects in a $Mg_{65}Cu_{25}Y_{10}$ bulk metallic glass. J Mater Sci 42(2):646
24. Regev M, Essel S, Katz-Demyanetz A (2017) Microstructure characterization of melt spun $Mg_{65}Cu_{25}Y_{10}$. Kovove Mater 55:1
25. Arison Kung RH, Ted Guo ML, Chang KF, Tsao CYA, Huang JC, Jang JSC (2018) Synthesis of Mg-Cu-Y bulk metallic glass plate via spray forming process. In: Proceedings of the 18th Int. AMME conference. https://doi.org/10.21608/amme.2018.34965
26. Ismail AI, Haliq R, Jamil M (2019) The study of crystallization of Mg-based bulk metallic glass (BMG). In: International conference on mechanical engineering research and application, IOP Publishing. https://doi.org/10.1088/1757-899x/494/1/012080
27. Rozenberg S, Audebert F, Galano M, Ogando IV, Mendive C (2016) Effect of Al addition to Rapidly Solidified Mg-Cu-Rare Earth Alloys. Mat. Res. 19:2
28. Ishitani T, Kaga H (1995) Transmission electron microscope sample preparation using a focused ion beam. J Electron Microsc 44:331
29. Men H, Kim WT, Kim DH (2004) Glass formation and crystallization behavior in $Mg_{65}Cu_{25}Y_{10-x}Gd_x$ (x=0, 5 and 10) alloys. J Non-Cryst Solids. 337(Suppl. 1):29
30. Xu F, Du Y, Gao P, Han Z, Chen G, Wang S, Jiang J (2007) Crystallization of melt-spun $Mg_{63}Ni_{22}Pr_{15}$ amorphous alloy ribbon. J. Alloys Comp. 441:76
31. Nagendra N, Ramamurty U, Goh TT, Li Y (2000) Effect of crystallinity on the impact toughness of a La-based bulk metallic glass. Acta Mater 48:2603
32. Zhou X, Ralston KD, Laws KJ, Cao JD, Gupta RK, Ferry M, Birbilis N (2013) Effect of the degree of crystallinity on the electrochemical behavior of $Mg_{65}Cu_{25}Y_{10}$ and $Mg_{70}Zn_{25}Ca_5$ bulk metallic glasses. Corrosion 69:781
33. Laws KJ, Gun B, Ferry M (2008) Large-scale production of $Ca_{65}Mg_{15}Zn_{20}$ bulk metallic glass samples by low-pressure die-casting. Mater Sci Eng, A 475:348
34. Chen G, Ferry M (2006) Crystallization and thermally induced surface relief effects in a $Mg_{65}Cu_{25}Y_{10}$ bulk metallic glass. J Mater Sci 42:646
35. Eshed E, Sc M (2013) Thesis. Technion, Haifa
36. Cullity BD (1978) Elements of X-ray diffraction, 2nd edn. Addison Wesley Publ. Comp. Inc., Reading, pp 416–420
37. Abrosimova GE, Aronin AS, Kholstinina NN (2010) On the determination of the volume fraction of the crystalline phase in amorphous-crystalline alloys. Phys Solid State 52:445
38. Sichina WJ (2000) PerkinElmer Instruments. https://thermalsupport.com/wp-content/uploads/2018/05/PETech-38.pdf
39. Gloriant T, Gich M, Surinach S, Baro MD, Greer AL (2000) Evaluation of the volume fraction crystallised during devitrification of Al-based amorphous alloys. Mater Sci Forum 343–346:365